

Polystyrene Nanopillars with Inbuilt Carbon Nanotubes Enable Synaptic Modulation and Stimulation in Interfaced Neuronal Networks


Ivo Calaresu, Jaime Hernandez, Rossana Rauti, Beatriz L. Rodilla, Ana Arché-Núñez, Lucas Perez, Julio Camarero, Rodolfo Miranda, M. Teresa González,* Isabel Rodríguez,* Denis Scaini,* and Laura Ballerini*

The use of nanostructured materials and nanosized-topographies has the potential to impact the performance of implantable biodevices, including neural interfaces, enhancing their sensitivity and selectivity, while reducing tissue reactivity. As a result, current trends in biosensor technology require the effective ability to improve devices with controlled nanostructures. Nanoimprint lithography to pattern surfaces with high-density and high aspect ratio nanopillars (NPs) made of polystyrene (PS-NP, insulating), or of a polystyrene/carbon-nanotube nanocomposite (PS-CNT-NP, electrically conductive) are exploited. Both substrates are challenged with cultured primary neurons. They are demonstrated to support the development of suspended synaptic networks at the NPs' interfaces characterized by a reduction in proliferating neuroglia, and a boost in neuronal emergent electrical activity when compared to flat controls. The authors successfully exploit their conductive PS-CNT-NPs to stimulate cultured cells electrically. The ability of both nanostructured surfaces to interface tissue explants isolated from the mouse spinal cord is then tested. The integration of the neuronal circuits with the NP topology, the suspended nature of the cultured networks, the reduced neuroglia formation, and the higher network activity together with the ability to deliver electrical stimuli via PS-CNT-NP reveal such platforms as promising designs to implement on neuro-prosthetic or neurostimulation devices.

1. Introduction

In the design of neural interfaces, nano-materials and nanostructured topologies are tools which may enable an improved interfacing with the nerve tissue. Nanotechnology-based engineering of neuronal interfaces aims at overcoming some of the current limitations of implantable devices, such as the mechanical matching with the central nervous system (CNS) tissue and the biological tolerance.^[1] Nanofabrication allows for bio-camouflage of interfacing electrodes via emulating extracellular matrix features, or allowing for 3D interfacing.^[2] Surfaces patterned with vertically aligned nanopillars (NPs) have been exploited as bio-interfaces.^[3] Mouse embryonic stem cells, neural progenitors, and hippocampal neurons, to name a few, were successfully cultured on NP substrates of different size, aspect ratio, shape, or density, with the aim to target the influence of surface topographical features on biological responses, including

Dr. I. Calaresu, Dr. R. Rauti,^[†] Dr. D. Scaini,^[††] Prof. L. Ballerini
International School for Advanced Studies (SISSA)
Trieste 265–34136, Italy
E-mail: dscaini@sissa.it; laura.ballerini@sissa.it

 The ORCID identification number(s) for the author(s) of this article can be found under <https://doi.org/10.1002/admi.202002121>.

© 2021 The Authors. Advanced Materials Interfaces published by Wiley-VCH GmbH. This is an open access article under the terms of the Creative Commons Attribution-NonCommercial-NoDerivs License, which permits use and distribution in any medium, provided the original work is properly cited, the use is non-commercial and no modifications or adaptations are made.

^[†]Present address: Department of Biomedical Engineering, Tel Aviv University, Tel Aviv 6997801, Israel

^[††]Present address: Department of Medicine, Imperial College London, Hammersmith Hospital, London SW7 2AZ, UK

Dr. J. Hernandez, Dr. B. L. Rodilla, Dr. A. Arché-Núñez, Dr. L. Perez, Dr. J. Camarero, Prof. R. Miranda, Dr. M. T. González, Dr. I. Rodríguez
Madrid Institute for Advanced Studies in Nanoscience (IMDEA Nanoscience)
C/Faraday 9
Ciudad Universitaria de Cantoblanco
Madrid 28049, Spain
E-mail: teresa.gonzalez@imdea.org; i.rodriguez@imdea.org

Dr. L. Perez
Dpto. Física de Materiales
Universidad Complutense de Madrid
Madrid 28040, Spain

Dr. J. Camarero, Prof. R. Miranda
Departamento de Física de la Materia Condensada and Instituto de Ciencia de Materiales Nicolás Cabrera
Universidad Autónoma de Madrid
Madrid 28049, Spain

DOI: 10.1002/admi.202002121

cell viability, proliferation, morphology, differentiation, adhesion, and motility.^[4–9] In this framework, conductive substrates made by, or enriched with, carbon-based nanomaterials (as carbon nanotubes [CNT] or graphene) have proved pivotal in interfacing nerve cells and studying their behavior.^[10–12]

In particular, for neuronal or progenitor cell cultures, NP patterned substrates have been designed to significantly influence proliferation and guidance, neural differentiation, outgrowth, and development.^[13,14] In the field of neuroscience, vertical nanowires or NPs have been shown to support the formation of axons in hippocampal neurons, and that of functional neuronal networks.^[8,15] Vertical nanowires have also been employed for single-cell stimulation and recording in experimental bioelectric interfaces.^[16] In most cases, NPs have been made out of hard materials like gallium phosphide semiconductors, silicon, or metals.^[15,17–19] Despite their remarkable features, semiconductors or metal NPs require long growth times and their production is time expensive. These materials are characterized by high Young's modulus which renders these NPs stiff and tedious to handle in bioassays, due to their fragility. Moreover, CNS tissues are soft, and as such, there is a substantial difference in stiffness between these NPs and the CNS tissues, leading to low mechanical compatibility. This mismatch in mechanical properties is believed to cause glia over proliferation and gliosis, once implanted *in vivo*.^[20] Polymeric, high aspect ratio, nanoscale topographies with a lower effective modulus would be more compliant with a good potential for improved biocompatibility.^[21]

Here, we developed an easy, affordable, and up-scalable fabrication strategy, based on nanoimprint lithography to pattern polystyrene (PS) surfaces with high-density and high aspect ratio NPs. Two different substrates were investigated: insulating NP surfaces (PS-NP), fabricated from pristine PS, and conductive NPs (PS-CNT-NP), produced from a PS nanocomposite where single-walled carbon nanotubes (SWCNTs) were used as conductive filler.

These NP substrates were optimized to support the development of primary neuronal cultures allowing the growth of planar neuronal circuits comprised of neural cells soma and axons, making functional synapse networks, and having a 3D exposure to the extracellular environment. We discovered that neuronal networks developed on NP substrates, compared to those grown on flat glass or flat PS surfaces, presented a reduction in glial cell density and a boost in spontaneous electrical activity. We suggest that these features result from the 3D-like microenvironment exposure of cells when suspended among NPs, emulating natural surroundings of cells as in *in vivo* conditions.

We successfully validated the possibility of using PS-CNT-NP to deliver electrical stimuli to the neural network and, finally, we showed that PS-NP and PS-CNT-NP were able to interface with and sustain the development of organotypic slices of mouse spinal cord.

2. Results and Discussion

2.1. Topography Fabrication and Characterization

Dense arrays of high aspect ratio NPs of 500 nm-diameter and 1 μm -pitch were selected as cell culture platforms to provide

a substrate topography where, due to the small spacing and size exclusion, interaction and adhesion of neuronal cells will be forced to take place only at the top of the topography (Figure 1).

An anisotropic square pillar arrangement was chosen rather than a compact hexagonal one to maximize interpillar space, ultimately filled by extracellular solution, while providing physical support for developing a planar neural network suspended at the top of NPs.^[4] NPs surfaces were prepared by soft thermal nanoimprint lithography (T-NIL). This technology allowed us to imprint NPs with the same dimensions in both insulating PS and in a PS/carbon-nanotubes composite (PS-CNT), thus providing precisely the same spatio-mechanical cue to the neuronal cells cultured on each of the substrates.

In Figure 1A, a scheme of the nanoimprint process is depicted, while Figure 1B shows a scanning electron microscopy (SEM) image of one of our high aspect ratio NP arrays (500 nm in diameter, 2 μm in height, in a square arrangement with a pitch of 1 μm). PS-NP substrates were produced by imprinting a PDMS working mold onto pristine PS films under optimum time, temperature, and pressure conditions (see Experimental Section for details). PS-CNT-NP substrates were produced in the same way by imprinting the NP structures on a composite material constituted by a PS matrix filled with single-wall carbon nanotubes (SWCNTs, 1% w/w).

Localized confocal Raman spectroscopy was performed to verify the presence of SWCNTs dispersed within the imprinted PS-CNT-NPs. Specifically, a laser light of 532 nm wavelength, providing a depth resolution of ≈ 400 nm, was utilized to detect the SWCNTs inside the NPs.^[22] Figure 1C compares the Raman spectra of pristine PS-NPs to PS-CNT ones, confirming SWCNTs' characteristics bands (D, G, and G'). This fingerprint is not present in pristine PS-NPs. The formation within the polymeric matrix of a percolation network of SWCNTs was confirmed by measuring the through-plane conductivity employing dielectric spectroscopy measurements (see Experimental Section). A value in the range of 10–100 mS cm^{-1} was measured for PS-CNT nanocomposite films.

Nanoindentation tests were conducted to determine the changes in surface stiffness upon patterning the substrates under study, and possibly identify a stiffness-dependent cellular adaptation on the different topographies.^[23]

Figure S1, Supporting Information, shows representative nanoindentation curves obtained from pristine PS, PS-NP, and PS-CNT-NP samples. The apparent stiffness (k), defined as the rate of change of probe depth with applied load, was determined from the slope of the unloading curves at the beginning of the loading–unloading nanoindentation cycles (elastic regime, low penetration values). The stiffness of the unstructured PS substrate ($1.6 \pm 0.15 \mu\text{N nm}^{-1}$) decreased by 84% after just surface (nano)patterning, and the apparent stiffness on the PS-NP topography set to values down to $0.25 \pm 0.03 \mu\text{N nm}^{-1}$. Upon the reinforcement of the PS-NP with SWCNT, the PS-CNT-NP patterned surface apparent stiffness increased slightly to $0.31 \pm 0.03 \mu\text{N nm}^{-1}$. These marked changes in the surface apparent stiffness can be inferred from the nanoindentation graphs displayed in Figure S1, Supporting Information.

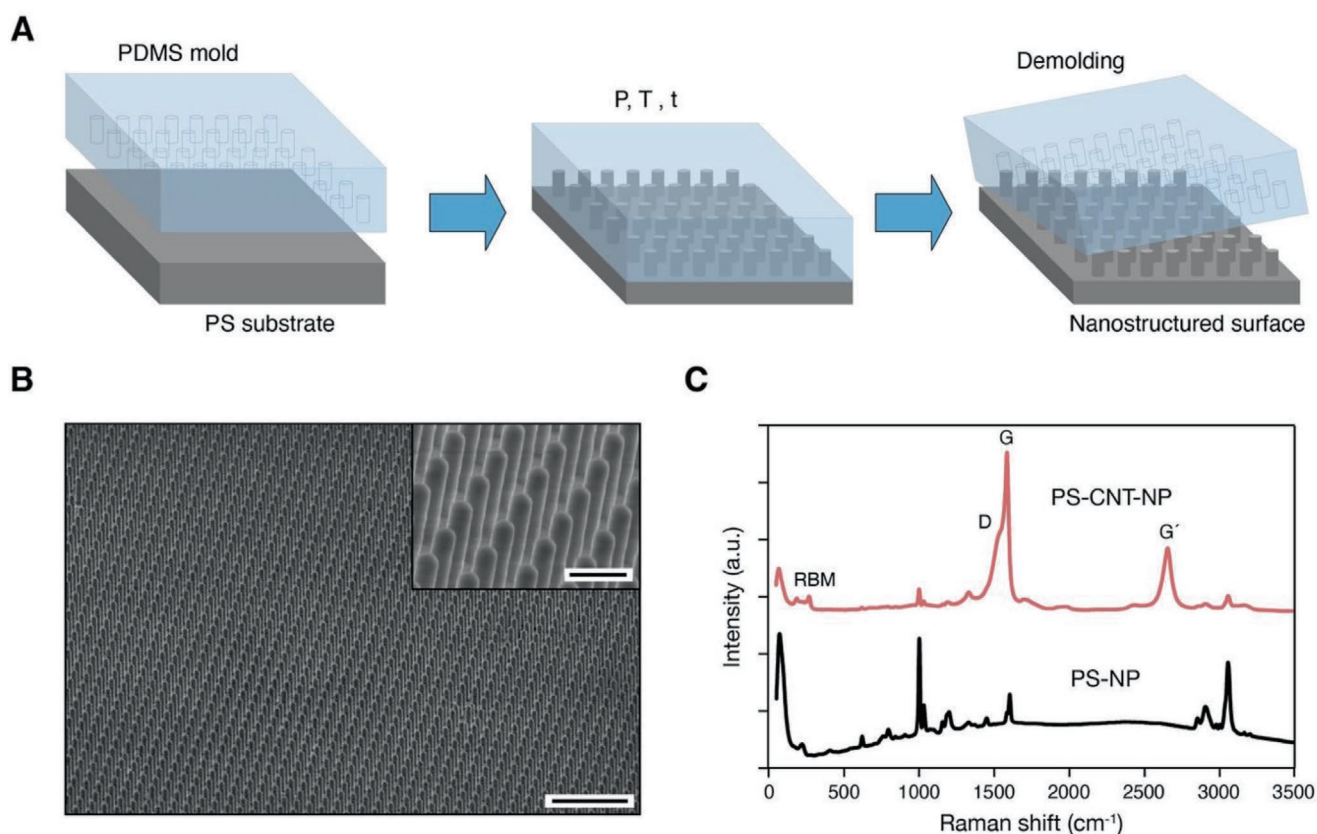


Figure 1. Fabrication and characterization of substrates patterned with polystyrene nanopillars (PS-NPs) and polystyrene-SWCNT nanopillars (PS-CNT-NP). A) Outline of the fabrication process of high aspect ratio nanometric pillar topography by nanoimprinting lithography. B) SEM images of a PS-CNT-NP imprinted substrate highlighting long-distance order and anisotropic square pillar arrangement. Image scale bar = 5 μm ; inset scale bar = 1 μm . C) Raman spectra obtained from both PS-NP and PS-CNT-NP topographies. The carbon nanotubes' characteristic D, G and G' peaks are visible in the PS-CNT-NP sample.

2.2. Characterization of Primary Hippocampal Cultures Interfaced to Nanopillar Substrates

In our first set of neurobiology experiments, we tested the stability of PS-NP (non-conductive and nanostructured) and PS-CNT-NP (conductive and nanostructured) once exposed to cells grown seeded on top of the NPs and submerged in cell culturing media for days. In particular, we investigated the substrates' ability to support neuronal adhesion and formation of neuronal networks. Neonatal rat hippocampal cells successfully adhered and grew on both substrates and were analyzed after 8–12 days *in vitro* (DIV; **Figure 2**), a time known to allow functional synaptic network development in *in vitro* conditions.^[24,25] The structural stability of both NP platforms, and their interaction with cultured hippocampal-cell soma, axons, and dendritic arborizations, were assessed by SEM. **Figure 2A** shows SEM micrographs at increasing magnifications (left to right) of control cells developed on poly-ornithine-coated glass coverslips (top row) and on the two nanostructured substrates (PS-NP and PS-CNT-NP, second and third rows, respectively). At low magnification (left panels), neuronal cell-bodies characterized by prominent neurites and glial cells branching are evident and appear in all three conditions. Higher magnification (**Figure 2A**, middle) reveals well-formed cell somas and neurites. At this

magnification, it is possible to appreciate that NPs are slightly tilted at cell-bodies' boundaries, suggesting cell's ability to exert peripheral tangential forces through focal adhesions engagement of the NPs heads and actomyosin-driven cytoskeletal contractions.^[26] These features are usually correlated to a healthy neuronal adhesion and growth.^[27,28] Further magnification (**Figure 2A**, right), allows visualizing distinct neuronal processes. NP substrates induced the formation of planar networks of neuronal processes apparently similar to those developed on controls. However, neurites ability to navigate by surfing on the top of NPs generated a suspended network architecture, whose axons and dendrites are exposed to the interpillars extracellular milieu with cell media flowing below as well on top of them (sketched in **Figure S4**, Supporting Information). We further investigated the size of the cultured networks and their cellular composition via immunofluorescence microscopy, labeling the specific cytoskeletal components β -tubulin III, to visualize neurons; 4',6-diamidino-2-phenylindole (DAPI), to highlight cell nuclei; and glial fibrillary acidic protein (GFAP) to visualize astrocytes (**Figure 2B**). We compared control, PS-NP, and PS-CNT-NP hippocampal networks morphology and cell composition. Control ($n = 77$, from five culture series), PS-NP ($n = 73$, five culture series), and PS-CNT-NP ($n = 80$, five culture series) showed a comparable density of β -tubulin III positive

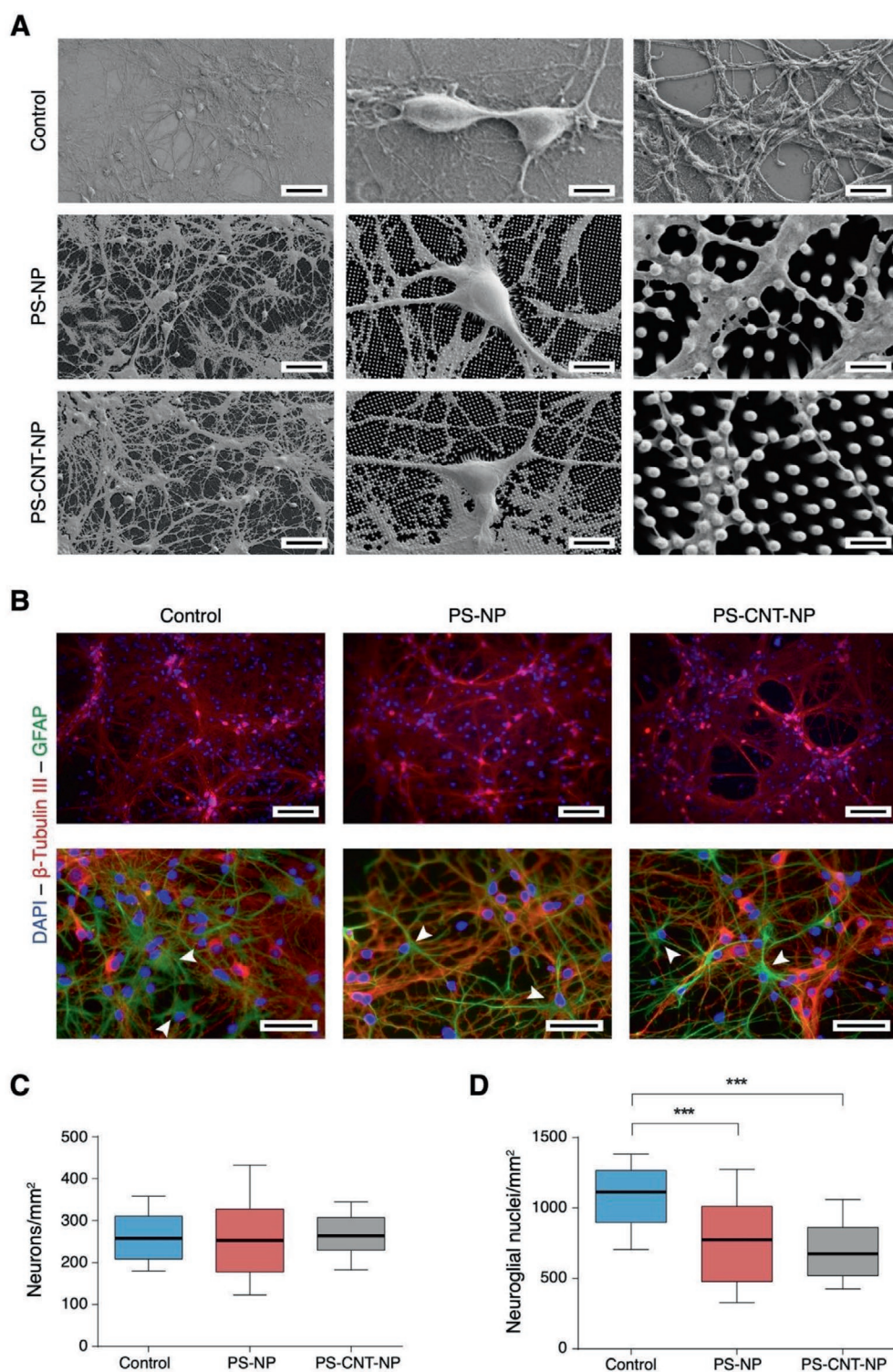


Figure 2. Morphology and cellular composition of hippocampal-cell networks developed on poly-L-ornithine-coated glass (control), polystyrene nanopillars (PS-NP), and polystyrene-SWCNT nanopillars (PS-CNT-NP). A) Scanning electron microscopy (SEM) images of dissociated hippocampal cultures grown (9 DIV) onto control, PS-NP, and PS-CNT-NP are shown at three increasing magnifications. Scale bars = 40, 10, and 2 μm from left to right. B) Epifluorescence micrographs of immune-labeled cultures for the three conditions. Neuronal cells are visualized, in the top images, by anti- β -tubulin III antibody (red), while all cellular nuclei were pointed out by DAPI staining (blue). Scale bar = 100 μm . On the bottom, enlarged representative fields show neurons in red (anti- β -tubulin III), astrocytes in green (anti-GFAP), and nuclei in blue (DAPI). Scale bar = 50 μm . C) Box plot summarizing neuronal densities for the three conditions. D) A box plot showing the densities of neuroglial cell nuclei (evaluated as the whole non-neuronal sub-population of cells in the samples; $***p < 0.001$).

neurons (highlighted in red in Figure 2B and quantified in the box plot in Figure 2C). The density of neuroglia cells, a heterogeneous population of cells that in the CNS includes oligodendrocytes, astrocytes, and microglia, was quantified from the same set of images as non-neuronal (i.e., β -tubulin III negative) stained nuclei (Figure 2B, top row; see Experimental Section). This measure pointed out a significant reduction in the overall number of glial cells on both PS-NP and PS-CNT-NP substrates (774 ± 347 and 675 ± 227 neuroglial cells/mm², respectively) when compared to control (1113 ± 249 neuroglial cells/mm²; $***p < 0.001$; box plot in Figure 2D). Interestingly, when we specifically focused on the astrocyte cell-phenotype (marked in green by GFAP in Figure 2B, bottom row), a substantial change in astrocyte morphology between flat and nanostructured substrates was qualitatively observed. In controls, astrocytes appear more spread and flatten than on both nanostructured substrates where they appear with a stellate shape (see arrows in Figure 2B, second row).

In a further set of experiments (four culture series) we selectively quantified the number of GFAP-positive cells comparing control, PS-NP, PS-CNT-NP, and PS-flat substrates, to rule out the possible contribution of PS per se (Figure S2, Supporting Information). Consistently with our first group of results, both flat substrates (PS-flat, $n = 46$ fields; and control, $n = 42$ fields) showed comparable astrocyte densities (297 ± 49 cells/mm² and 274 ± 54 cells/mm², respectively), while in the nanostructured substrates (PS-NP, $n = 45$ fields, and PS-CNT-NP, $n = 45$ fields) GFAP positive cells density was significantly reduced (199 ± 42 cells/mm² and 138 ± 51 cells/mm², respectively; $***p < 0.001$). No difference was depicted in neuronal densities comparing PS-flat substrates with the other conditions (results summarized in Figure S2A,B, Supporting Information).

We suggest that the decrease in glial cell density brought about by NP-structured substrates may be ascribed to mechanisms related to the cell focal contact modulation by the topography and related mechanotransduction processes.^[29–32] In addition, other features such as the reduced apparent stiffness of the nano-topographies may induce this cellular response.^[33] Furthermore, a reduced glial cell proliferation may have been favored by the suspended configuration these cultures adopt in the high aspect ratio topography. In any case we can rule out a mere inhibition of proliferation due to the PS chemical characteristics since the behavior is not consistent in all the substrates being made of the same polymer matrix. Regardless of the mechanisms reducing glial cells adhesion/proliferation on NPs substrates, this feature might imply a lower reactive gliosis when interfacing CNS tissue with the NP substrates.^[21,34]

2.3. Nanopillars-Based Substrates Increase Synaptic Network Performance

Upon ex vivo reorganization of synaptic networks, primary cultured neurons display spontaneous and temporally structured electrical activity.^[35,36] We explored the network dynamics in control, PS-NP, and PS-CNT-NP hippocampal cultures (9–12 DIV; five culture series) by fluorescent imaging with calcium

indicators (Figure 3). This is a minimally invasive approach that allows monitoring neuronal activity following the calcium transients occurring in a neuronal network at a single-cell level.^[37] Living neurons, stained with the membrane-permeable dye Oregon Green 488-BAPTA-1 AM, were visualized within randomly chosen sample areas ($660 \times 660 \mu\text{m}^2$, Figure 3A, left images) and, on average, 135 ± 30 fluorescent cells were analyzed for each experimental condition (see Experimental Section).

In all culture groups, we detected spontaneous and repetitive calcium events emerging from episodes of synaptic, action potential-dependent, bursts of activity (Figure 3A, tracings). This electrical activity was entirely blocked by tetrodotoxin (TTX, $1 \mu\text{M}$; a blocker of fast voltage-gated Na⁺ channels) applications, demonstrating its dependence upon neuronal firing and synaptic activation (Figure 3A, right traces).^[37] We quantified spontaneous calcium episodes in active cells by measuring the interevent interval (IEI), the time interval between the onset of a calcium burst and the beginning of the next one. IEI values were significantly reduced (thus activity increased) in PS-NP and PS-CNT-NP substrates compared to control ones (results summarized in the box plot of Figure 3B; $***p < 0.01$ and $***p < 0.001$, respectively, for control vs PS-NP and control vs PS-CNT-NP). Network activity was not affected by PS-flat, again ruling out a role of PS per se (Figure S2C, Supporting Information, left traces). A distinct feature of network dynamics is the emergence of synchronized calcium events in cells located within the same field of view. We quantified this parameter by measuring the correlation coefficient function (CCF) among pairs of cells (Figure S3, Supporting Information, see Experimental Section for details). Neurons displaying a Pearson CCF that was significantly larger than that expected by chance, were considered positively correlated. The bar plot in Figure 3C shows that in control $46 \pm 1\%$ of cell pairs ($n = 661$ pairs) were positively correlated; this value rose to $86 \pm 2\%$ and $96 \pm 2\%$ in PS-NP ($n = 876$ pairs) and PS-CNT-NP ($n = 983$ pairs), respectively.

To investigate the mechanism responsible for the increased activity observed in NP substrates, we performed single neuron, whole-cell, patch-clamp recordings directly comparing synaptic activity recorded in flat substrates (control) with the nanostructured ones (PS-NP) (Figure 4).

Figure 4A shows current tracings characterized by heterogeneous events of inward currents which represent basal spontaneous synaptic activity of a control neuron and a PS-NP one.^[24] No significant variations in the mean amplitude values of the post-synaptic currents (PSCs) was measured between the two conditions ($n = 11$ cells for control, $n = 17$ cells for PS-NP). Conversely, we detected a significant increase ($***p = 0.009$) in the PSCs frequencies when comparing the two conditions (control: 0.9 ± 0.3 Hz; PS-NP: 2.1 ± 0.4 Hz; Figure 4A, right box plot), confirming the presence of increased network activity in NP cultured neurons. In Figure 4B we recorded miniature PSCs (mPSCs) in the presence of TTX ($1 \mu\text{M}$) in both control and PS-NP conditions. Recording mPSCs allows disambiguating dynamical from structural changes of neural circuit activity. mPSCs, in fact, reflect the stochastic release of vesicles from the presynaptic terminals and mPSC frequency depends on the number of synaptic contacts, while their amplitude depends on

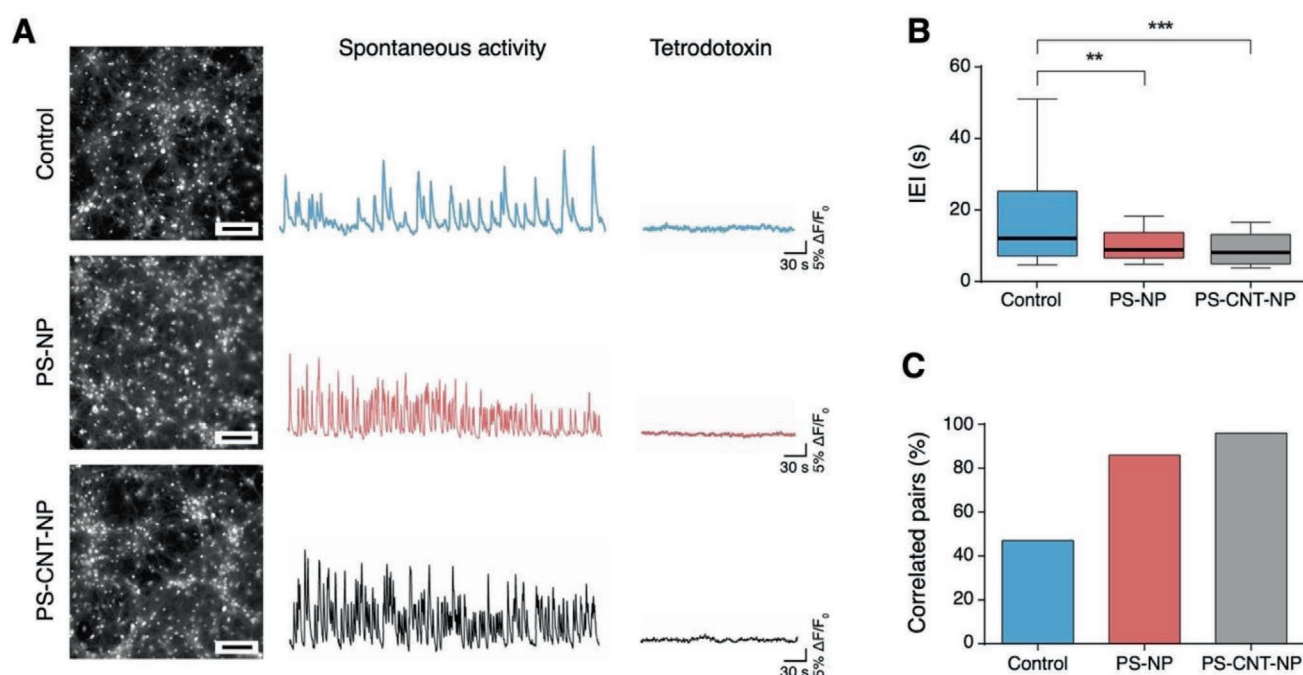


Figure 3. Calcium imaging experiments were used to monitor spontaneous network activity onto control, PS-NP, and PS-CNT-NP samples. A) Snapshots of three representative fields of hippocampal dissociated cultures labeled with Oregon Green 488-BAPTA-1 AM. Scale bar = 100 μm . Active cells were manually selected as regions of interest (ROI) from which calcium variations were evaluated. Representative traces for each condition are shown (central traces). Tetrodotoxin was used at the end of each recording to assess the neuronal nature of the signals (right traces). Calcium transients are expressed as fractional amplitude increase ($\Delta F/F_0$). B) Cells grown onto nanopillars exhibited enhanced spontaneous activity depending on substrate topography (** $p < 0.01$). C) In the bar chart, the percentages of correlated cell pairs were plotted for each condition. Bars represent the percentage of significantly correlated pairs over the total amount of cell pairs analyzed. Calcium events correlation raised from 46% in control cultures to 86% and 96% in nanopillars cultures (PS-NP and PS-CNT-NP, respectively).

post-synaptic receptor sensitivity.^[38] In these experimental conditions, we did not detect any significant variation in mPSCs mean amplitude values ($n = 8$ cells for control, $n = 9$ cells for PS-NP). Instead, we measured a significant increase ($p = 0.012$) in mPSCs frequencies when comparing control to PS-NP samples (0.6 ± 0.2 vs 1.6 ± 0.3 Hz, respectively; Figure 4B, right box plot). In all recordings we never detected changes in neuronal passive membrane properties (for capacitance, control: 84 ± 33 pF; PS-NP: 97 ± 32 pF; $p = 0.20$; and input resistance, control: 436 ± 211 M Ω ; PS-NP: 361 ± 190 M Ω ; $p = 0.22$; Figure 4C).

To estimate whether changes in synaptic density may account for the enhanced mPSC frequency observed in NP neurons, cultured hippocampal neurons were coimmunostained for β -tubulin III, DAPI, and the synaptic marker Bassoon.^[39]

We quantified the number of synaptic contacts in the two conditions evaluating the volumetric ratio between Bassoon's presynaptic marker, which labels the presynaptic active zone, and the neuronal tracer β -tubulin III. Results are summarized in the box plot in Figure 4E, where a significant increase in synaptic-related signal is evincible in PS-NP samples in comparison to the control condition (control: 0.06 ± 0.01 ; PS-NP: 0.16 ± 0.01 ; $n = 23$ and 25 , respectively; $p = 0.0015$). All results presented so far indicate that synaptogenic processes are facilitated in neuronal networks developed above NP-surfaces, that is in the suspended bidimensional configuration.

2.4. Carbon-Based Nanostructures as a Platform for Effective Electrical Neurostimulation

We further evaluated the possibility of exploiting our conductive nanostructured substrates (PS-CNT-NP) as a neurostimulating platform (Figure 5). We monitored neuronal responses during electrical stimulation through PS-CNT-NP with a two-electrode system.^[40] For this purpose, we used the experimental setup sketched in Figure 5A, where a PS-CNT-NP surface was exploited concurrently as culturing substrate and planar working electrode against an Ag/AgCl pellet reference electrode, both placed in the physiological saline solution. The emergence of evoked neuronal activity upon external electrical stimulation was monitored via real-time calcium imaging visualization.^[41,42] Spontaneously active neurons were selected and pharmacologically decoupled from the network by a cocktail of receptor antagonists (APV/CNQX/bicuculline, see Experimental Section for details), to block ionotropic glutamate receptors subtypes and GABA_A ones (Figure 5B). In the presence of these blockers, synaptic activity was silenced, thus burst of activity in neurons could only be detected when evoked by direct electrical stimulation via the CNT NPs.^[43,44] We tested a stimulation protocol where five consecutive cathodic voltage squared pulses at 0.2 Hz (1 V mm^{-2} , train-to-train frequency = 0.01 Hz) were delivered by the PS-CNT-NP extracellular surface/electrode (Figure 5C). As shown in Figure 5D (top calcium imaging trace), such a stimulation

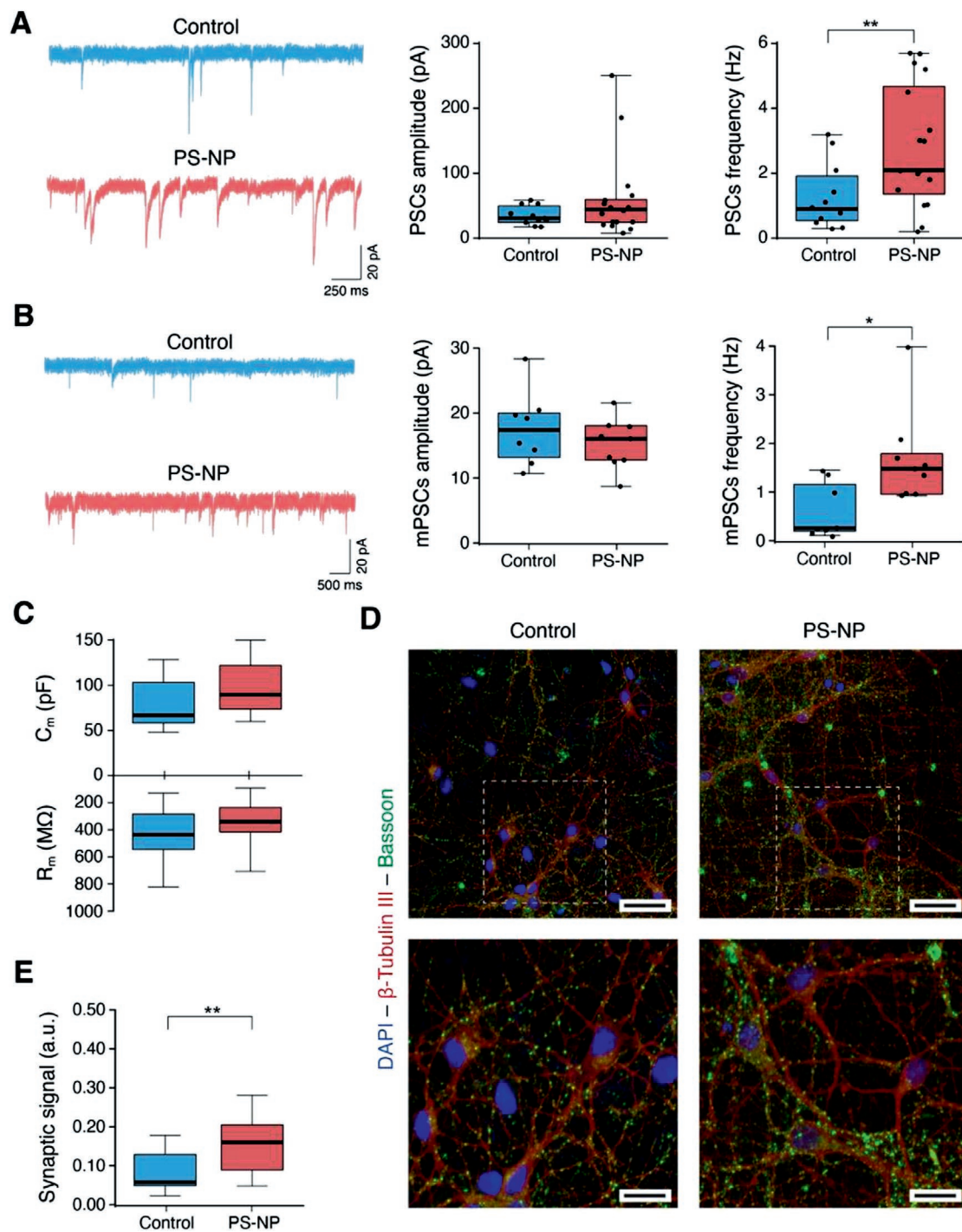


Figure 4. Synaptic modifications of nanopillars-interfaced neurons. A) Representative spontaneous post-synaptic currents (PSCs) tracings of patch-clamped neurons onto control and PS-NP are shown together with the box plots summarizing amplitude (left) and frequency (right) of the spontaneous PSCs. We superimposed to the plots the scattered distribution of the data to give a better sense of values distribution (each dot representing a different cell). Comparably to what was observed during calcium imaging experiments, spontaneous synaptic activity was boosted by PS-NP (** $p < 0.01$). B) Representative tracings of miniature post-synaptic currents (mPSCs) recorded in the presence of $1 \mu\text{M}$ TTX are provided with their amplitude and frequency box plots (left and right respectively, scattered distribution of values superimposed; each dot representing a different cell). Note the increased miniature currents frequency of PS-NP neurons (* $p < 0.05$). C) Passive membrane properties of neurons were comparable in control poly-L-ornithine-coated glass and polystyrene nanopillars (PS-NP). D) Confocal Z-projection of fluorescent micrographs at two increasing magnifications was reconstructed to show synapse-labeled cultures grown onto control and PS-NP. Increased synaptic clustering onto PS-NP can be observed by the greater Bassoon (green) reactivity, while neuronal cells are visualized by anti- β -tubulin III antibody (red), and nuclei are marked with the classical DAPI staining (blue). Scale bar = 25 and 10 μm . E) The box plot showing the fraction of neuronal volume occupied by synaptic clusters summarizes such an observation (** $p = 0.0015$).

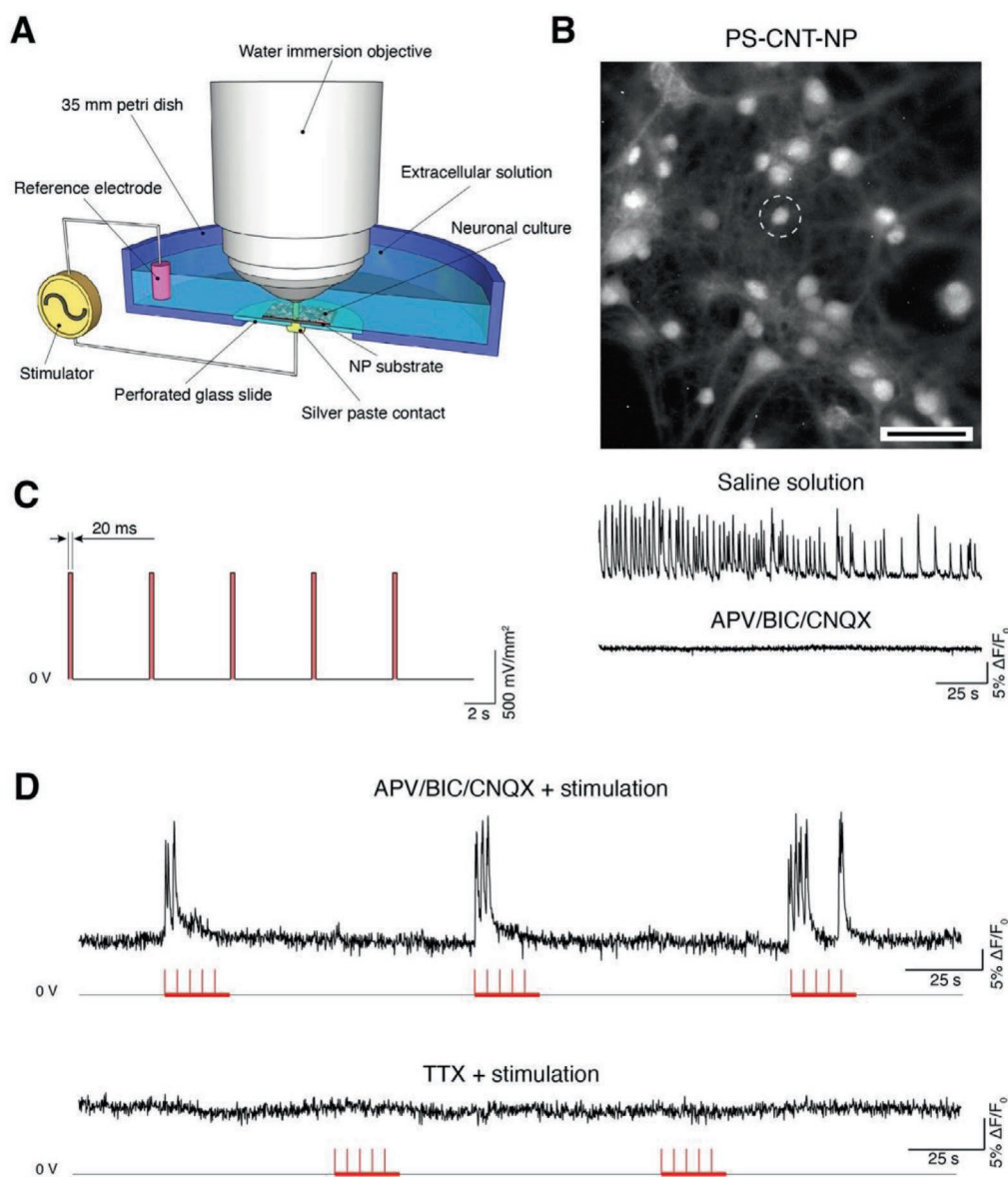


Figure 5. Electrical stimulation from conductive PS-CNT nanopillars composite. A) A sketch of the experimental setting used to electrically stimulate neuronal tissues through our PS-CNT-NP substrates is depicted. B) A snapshot of a representative field of hippocampal dissociated cultures grown onto PS-CNT-NP and labeled with Oregon Green 488-BAPTA-1-AM (Scale bar = 50 μm). Typical recordings of spontaneous synaptic activity monitored via live calcium imaging are shown below in the case of saline solution perfusion (top trace), and in the presence of the APV/BIC/CNQX silencing cocktail (bottom trace). C) Schematic of the stimulation protocol used: it consists of three stimulation trains (0.01 Hz) of five voltage steps (1 V mm^{-2} and 20 ms in amplitude and duration, at 0.2 Hz). D) A representative trace showing the neuronal response in the presence of a cocktail of synaptic blockers; in this condition, the network is silenced, and only evoked activity could be visible (top trace). The red lines correspond to the 25 s-long pulse trains; the strong increase in Ca^{2+} fluorescence during NP stimulation is noticeable. Such responses were entirely abolished by tetrodotoxin administration (bottom trace), thus confirming the neuronal nature of the detected signals, and indicating that evoked action potentials triggered such a rise in Ca^{2+} . Calcium transients are expressed as fractional amplitude increase ($\Delta F/F_0$).

reliably evoked calcium bursts that were abolished by TTX (see Experimental Section) administration (Figure 5D, bottom trace), thus confirming the neuronal origins of the observed signals and the ability of PS-CNT-NP substrates to interface the neuronal network electrically. Such a phenomenological observation suggests that PS-CNT-NP platforms might represent a reliable interface to physically and electrically interface neuronal tissues.

2.5. Nanopillars Interfacing to a Complex Tissue

Cultured CNS explants provide an *in vitro* model of a complex neuronal network. In the last set of experiments, we decided to validate the long-term biological tolerance of nanostructured substrates (i.e., PS-NP and PS-CNT-NP) by interfacing them with spinal cord organotypic cultures for weeks. Organotypic spinal slices represent a biological model of segmental microcircuits

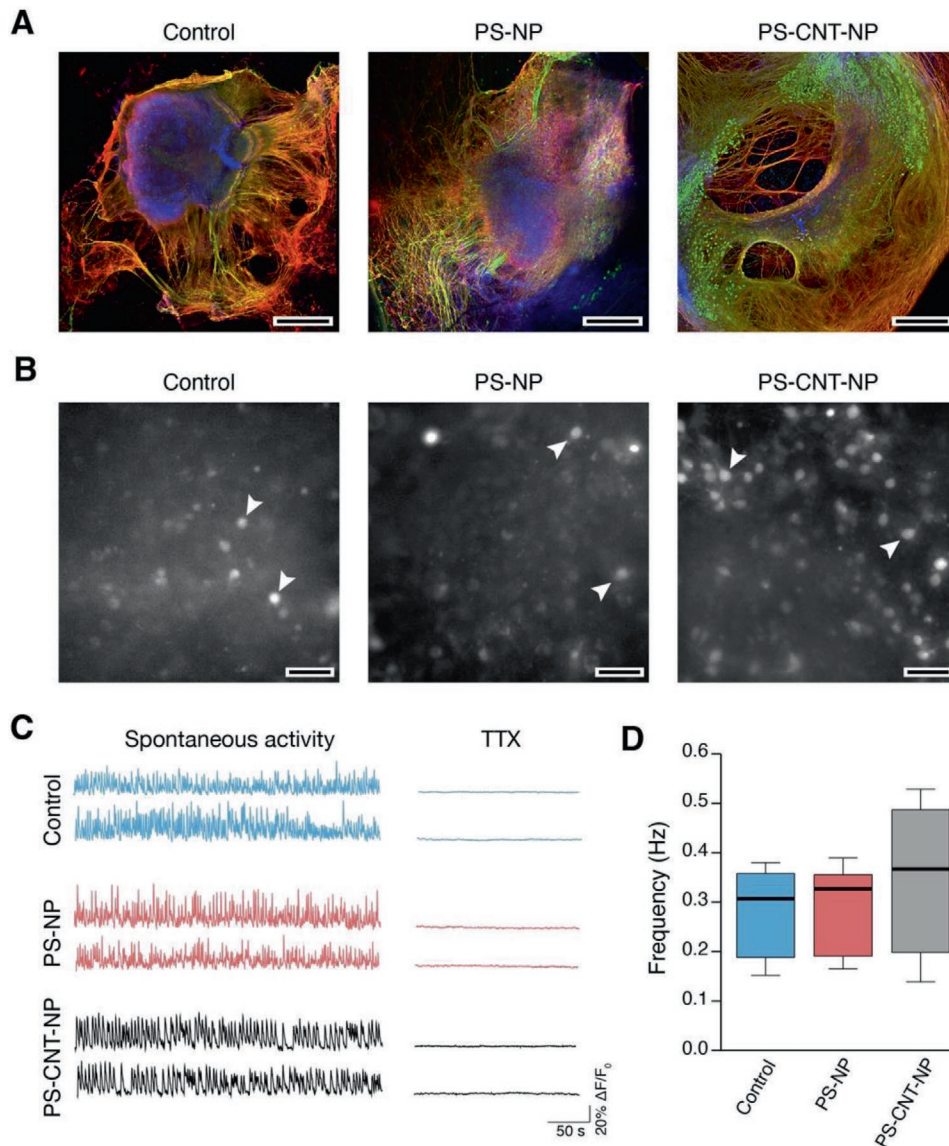


Figure 6. Organotypic spinal cord slices development onto polymeric nanopillars. A) Three low-magnification confocal stitching of transversal spinal cord slices grown for 21 DIV are depicted. Neurons are visualized with an anti- β -tubulin III antibody (red), specific motoneuron labeling is achieved with SMI-32 (green), while cell nuclei are targeted by DAPI staining (blue). Scale bar = 500 μ m. B) Representative snapshots of the ventral regions relative to the three substrates after spinal cord slices were loaded with the Ca^{2+} -dye Fluo-4 AM. Scale bar = 50 μ m. C) Two representative traces (from the highlighted couple of neurons in panel [B]) of the recorded motoneuronal spontaneous activity are given for every condition (left traces). Tetrodotoxin was used at the end of each recording to assess the neuronal nature of the signals (right traces). Calcium transients are expressed as fractional amplitude increase ($\Delta F/F_0$). D) The box plot summarizes calcium-spiked frequency (Hz) during spontaneous motoneurons activity.

which is maintained in *in vitro* conditions for weeks (Figure 6).^[45] We used immunofluorescence labeling and confocal microscopy to study the adhesion, development, and final morphology of explanted spinal tissues and their axonal regrowth when chronically interfaced to PS-NP, PS-CNT-NP, and control substrates for 21–24 DIV (see Experimental Section for details). Immunofluorescence confocal images at low magnification of the three conditions are depicted in Figure 6A. It is possible to note the healthy and complex structure of the spinal explants when grown interfaced with the three substrates. The entire spinal cross section is visible including the spinal slice, at the center, the peripheral dorsal root ganglia, and a dense mesh

of neurites in the surrounding outgrowth belt, highlighted by β -tubulin III positive neurites (in red) and the specific antibody against axonal neurofilament H (SMI-32, in green). No alterations in the growth and morphology of explanted spinal cord cultures were observed between the three conditions.

We further tested the functional impact of interfacing spinal slices on both nanostructured substrates. Organotypic spinal cord slices exhibit an intense spontaneous synaptic activity, monitored via live calcium imaging as spontaneous bursts emerging as irregular synchronized firing epochs (Figure 6B,C).^[46] Fluorescent cells can be observed within the ventral area (premotor area) of each slice culture (arrows in

Figure 6B). Spontaneous neuronal activity was measured by simultaneously imaging the intracellular calcium dynamic of selected neurons; these transients were fully blocked by TTX application demonstrating their neuronal origin (left and right traces in Figure 6C). Spontaneous calcium episodes were analyzed, and the resulting frequency (in Hz) was highly conserved between all tested conditions (Figure 6D). This result provides evidence of an appropriate maturation and development of the spinal cord slice when interfaced to nanostructured substrates.

The absence of a substantial increase in the electrical activity in suspended slices when compared to dissociated hippocampal cultures might be due to the different CNS anatomical origin (spinal cord vs cortex) and by the long-term interfacing of organ cultures, leading to homeostatic adjustments of neuronal activity.^[47]

Indeed, differently from a newly formed network of dissociated neurons, organotypic slices are characterized by complex 3D cytoarchitecture governing the electrophysiological behavior of the network. The resulting robust network activity, reflecting the spinal activity of the original tissue, might be more difficultly altered in the long term by the NP structure.

3. Conclusion

We successfully developed insulating and conductive high aspect ratio NP-based interfaces, constituted by cylindrical structures of 500 nm in diameter square-organized with a pitch of 1 μm , able to successfully support the development of healthy and functional neuronal networks characterized by a suspended topology. These networks show similar cellular organization and neuronal cell content of control cultures, but a significant reduction in the densities of astrocyte cellular population. This is not due to the mere chemical nature of PS but, more likely, to the combined effect of the surface (nano)morphology and the reduced apparent stiffness of the substrate compared to flat PS surfaces. In addition, the suspended organization of cultured cells might discourage the formation of glial layers interposed between the substrate and the neuronal cells.^[48] This supportive cell layer could be less needed to the circuit formation due to the nanostructured surfaces of NP inducing submicrometrical surface adhesivity.

Valuably, both the tested substrates (PS-NP and PS-CNT-PS) allowed the development of suspended networks, characterized by increased network activity and higher degree of synchronization among cells pairs. It is tempting to speculate that, in the case of dissociated cultures, this configuration mimics the exposure of cell membrane (Figure S4, Supporting Information, left) to a 3D geometry, providing neurons and neuronal connections with an improved efficiency, due to their accessibility to the third dimension.^[37,49]

Finally, we validated these novel conductive nanostructured substrates (PS-CNT-NP) as a reliable device to electrically interface neural tissues demonstrating the possibility to elicit electrical activity, in the form of evoked calcium bursts, by extracellular stimulation of the conductive NPs. With the possible application of our nanostructured surfaces as a neuroelectric interface for in vivo stimulation in mind, we validated PS-NP's

and PS-CNT-NP's ability to support the long-term growth in vitro of spinal cord explants.

These experiments opens the possible applicability of our high aspect ratio PS-NP and, more interestingly, our PS-CNT-NP patterned substrates as a nerve tissue interfacing platform, with the advantage of inducing low gliosis, preserving intact tissue physiological activity, and the possibility to effectively electrically stimulate the nervous tissue.

4. Experimental Section

Fabrication and Characterization of High Aspect Ratio Nanopillar Substrates: The PS-CNT nanocomposites films with $\approx 1\%$ w/w of functionalized single-wall carbon nanotubes (P3-SWCNT, Carbon Solutions Inc.) were prepared beforehand by solution blending, which was a commonly used method for the preparation of polymer-carbon nanotubes nanocomposites.^[50] Briefly, a stable dispersion of SWCNT was initially prepared in toluene (99.8%, Acros Organics) by tip-sonication. A fixed volume of the dispersion was subsequently added to a PS solution prepared in toluene too. Using a dispersion tool (Ultra-Turrax, 10 000 rpm), three stirring-sonication cycles were carried out to ensure good mixing and dispersion. Next, the nanocomposite was coagulated by the dropwise addition of the solution to cold methanol (reagent grade, Scharlau) under intense stirring. The obtained precipitate was filtered using a Buchner funnel, repeatedly washed with methanol, and dried in vacuum at 80 $^{\circ}\text{C}$ overnight. 200–300 μm -thick self-standing PS and PS-CNT films were obtained by melt pressing using a hydraulic press with heating plates adapted (Specac Atlas 15T, temperature set at 140 $^{\circ}\text{C}$ and pressure at 10 tons).

PDMS molds with a pore size of 500 nm in diameter and 2 μm in length obtained from a silicon master by soft lithography, were used to fabricate high aspect ratio nanostructured substrates by T-NIL, employing an EITRE Nano Imprint Lithography system (Obducat AB, Sweden). The thermal imprinting conditions were $T = 130$ $^{\circ}\text{C}$, $P = 30$ bar and $t = 5$ min for pristine PS and $T = 140$ $^{\circ}\text{C}$; $P = 30$ bar, $t = 5$ min for the SWCNT nanocomposite (PS-CNT).

A confocal Raman microscopy (SENTERRA, Bruker) was employed to verify the dispersion and penetration of the SWCNT into the NPs working at wavelengths of 532 and 785 nm.

The NPs' apparent stiffness was evaluated by performing nanoindentation tests using a Hysitron TI-950 TriboIndenter employing a diamond probe with a tip radius of 10 μm . Nanoindentations measurements were performed by making 20 load-hold-unload cycles (1 s/segment) on different areas of the imprinted substrates. Unloading values up to 50% were employed in each cycle until a maximum load of 40 μN was reached. The minimum critical buckling load for uniaxial compression was estimated through the geometrical parameters of an individual pillar to be ≈ 25 μN , assuming a modulus of 3.2 GPa for the PS (according to manufacturer specifications).

The through-plane conductivity of the nanocomposites was evaluated by broadband dielectric spectroscopy using a Novocontrol broadband dielectric spectrometer. 10 mm-diameter gold electrodes were first deposited by sputtering on both surfaces before the measurements.

Primary Cultures: Dissociated hippocampal neurons were obtained from P2–P3 old Wistar rats, as previously reported.^[24,25] All procedures were approved by the local veterinary authorities and performed in accordance with the Italian law (decree 26/14) and the UE guidelines (2007/526/CE and 2010/63/UE). Animal use was approved by the Italian Ministry of Health (no. 22DABNQYA). All efforts were made to minimize suffering and to reduce the number of animals used. PS-flat, PS-NP, and PS-CNT-NP substrates were carefully rinsed with three 5 min-long washes with Milli-Q water (Merck Millipore). Samples were therefore dried at 60 $^{\circ}\text{C}$, and their surfaces were activated under a low-pressure air plasma (Harrick PDC-32G Plasma Cleaner) for 7 min at room temperature, with a radiofrequency coil power set to 9 W.

A 20 min-long exposition to UV-radiation was finally used to sterilize the substrates immediately before cell plating.^[51] About 800 cells/mm² were plated onto poly-L-ornithine-coated (Sigma-Aldrich) glass coverslips (control), PS-flat, PS-NP, and PS-CNT-NP substrates, and incubated at 37 °C; 5% CO₂ in Neurobasal medium (Invitrogen) was added with B-27 supplement (Thermo Fisher) and GlutaMAX (Thermo Fisher) both to a 1× final concentration. Gentamicin (Thermo Fisher) was also added to a final concentration of 5 μg mL⁻¹ to prevent contamination. Cultured cells were grown until 8–12 days in vitro (DIV) by renewing half of the medium once in this period.

Immunocytochemistry and Fluorescent Microscopy: Cultures were fixed in 4% formaldehyde, prepared from fresh paraformaldehyde, in PBS 1× and permeabilized for 30 min with 0.3% Triton-X-100 (Carlo Erba) in PBS 1× added with 5% FBS (Gibco) and 4% BSA (Sigma-Aldrich) to prevent non-specific binding of primary antibodies. Samples were subsequently incubated with primary antibodies for 30 min at room temperature and, after being washed with PBS 1×, with secondary antibodies for 45 min. Mounting was performed with antifade medium Fluoromount (Sigma-Aldrich) on 1 mm-thick microscope glass slides. Neurons were labeled through anti-β-tubulin III primary antibody (1:800, Sigma-Aldrich) and visualized with Alexa 594 antirabbit in goat as the secondary antibody (1:800, Invitrogen). Astrocytes were instead stained with mouse anti-GFAP primary antibodies (1:800, Sigma-Aldrich) and visualized with Alexa 488 antimouse in goat as the secondary antibody (1:800, Invitrogen). Nuclei were stained with DAPI (1:800, Invitrogen). To estimate neurons and astrocytes number, images of immunolabeled cultures were acquired using a Leica DM6000 Epifluorescence Microscope, either using 10× or 20× objectives (HC PL Fluotar, 0.30 NA and 0.50 NA, respectively). The authors collected eight to ten fields per culture in two cultures per series from four to five different culture series. The total number of nuclei in each field and the number of neurons and astrocytes were manually counted. Image analysis and reconstruction were accomplished using NIS-Elements (Nikon) and ImageJ (NIH) software.

Scanning Electron Microscopy: The interaction between neurons and pillars was qualitatively assessed through SEM. Images were acquired collecting secondary electrons on a Gemini SUPRA 40 SEM (Carl Zeiss NTS GmbH, Oberkochen, Germany). Primary cultures onto PS-NP and PS-CNT-NP were fixed in with 2% glutaraldehyde dissolved in cacodylate buffer (0.1 M, pH 7.2) in the dark for 1 h at room temperature. After fixation, samples were carefully rinsed with cacodylate buffer; the dehydration process followed by dipping the sample in water/ethanol solutions at progressively higher alcohol concentrations (50%, 75%, 95%, and 100% ethanol for 3 min each). Samples were left to dry overnight at 4 °C temperature in the dark. Before SEM imaging, samples were metalized in a metal sputter coater (Polaron SC7620). Cells were visualized at low accelerating voltages (1–2 keV) to prevent electron-induced surface charging.

Calcium Imaging: Hippocampal dissociated cultures were loaded with cell-permeable Ca²⁺ dye Oregon Green 488 BAPTA-1-AM (Molecular Probes); 10 μL DMSO (Sigma-Aldrich) was added to the stock 50 μg of the dye, and cultures were incubated with a final concentration of 4 μM for 30 min at 37 °C, 5% CO₂. Samples were therefore placed in a recording chamber mounted on an inverted microscope (Nikon Eclipse Ti-U). Cultures were continuously perfused at 5 mL min⁻¹ rate and room temperature with an extracellular saline solution of composition (× 10⁻³ M): 150 NaCl, 4 KCl, 2 CaCl₂, 1 MgCl₂, 10 HEPES, and 10 glucose (pH adjusted to 7.4 with NaOH; osmolarity ≈ 300 mOsm). Ca²⁺-dye was excited at 488 nm with a mercury lamp; excitation light was attenuated using an ND filter (1/32) and separated from the light emitted from the sample using a 505 nm dichroic mirror. Oregon-loaded cultures were observed with a 20× objective (PlanFluor, 0.45 NA), and images were continuously acquired (exposure time 150 ms) using an ORCA-Flash4.0 V2 sCMOS camera (Hamamatsu). The imaging system was controlled by an integrated acquisition software (HCLImage Live), and the camera was set to operate on 2048 × 2048 pixels² at binning 4. Cultures were accustomed to extracellular solution for ≈10 min. Spontaneous activity was, therefore, recorded for 10 min. 10 μM bicuculline (GABA_A antagonist; Sigma-Aldrich) was subsequently perfused for 20 min

to weaken the synaptic inhibition and increase the synchronization. Finally, 1 μM TTX (a voltage-gated, fast Na⁺ channel blocker; Latoxan) was added to confirm the recorded signals' neuronal nature. The authors recorded one field from each sample, and 15 ± 2 cells from each recording were selected by drawing regions of interest around cell-bodies (*n* = 9 cultures from five different series). Images were analyzed with ImageJ software (NIH), and the corresponding traces were studied with Clampfit software (pClamp suite, 10.4 version; Axon Instruments) in off-line mode and with MATLAB (MathWorks, Inc.). The difference between consecutive peaks onset times was computed, to obtain the IEI. Intracellular Ca²⁺ transients were expressed as fractional amplitude increase ($\Delta F/F_0$, where F_0 is the baseline fluorescence level and ΔF is the rise over baseline); the onset time of neuronal activation was determined by detecting those events in the fluorescence signal that exceed at least five times the standard deviation of the noise.^[37] Cross-correlation analysis was performed following the methodology described by S. Usmani et al., 2016.^[51]

Electrophysiology: Patch-clamp, whole-cell, recordings were achieved with glass micropipettes with a resistance of 4–7 MΩ. The patch micropipette was filled with intracellular solution containing: 120 × 10⁻³ M K-gluconate, 20 × 10⁻³ M KCl, 10 × 10⁻³ M HEPES, 10 × 10⁻³ M EGTA, 2 × 10⁻³ M MgCl₂, and 2 × 10⁻³ M Na₂ATP; pH 7.3. Cultures were positioned in a custom-made chamber mounted on an inverted microscope (Eclipse TE-200, Nikon, Japan) and continuously superfused with the extracellular solution as in calcium imaging experiments. Cells were voltage-clamped at a holding potential of -56 mV (not corrected for liquid junction potential, calculated to be -13.7 mV at 20 °C in the experimental conditions), and spontaneous PSCs were recorded. mPSCs were recorded in the presence of the fast voltage-gated Na⁺ channels blocker TTX (1 μM; Latoxan). Data were collected at a sampling rate of 10 kHz using a Multiclamp 700A patch amplifier (Axon CNS, Molecular Devices LLC, US) connected to a PC through a Digidata 1440 (Molecular Devices LLC, US). Input resistance and cell capacitance were measured off-line using Clampfit 10.4 software suite (Molecular Devices LLC, US), while spontaneous and miniatures PSCs were analyzed in Axograph (Axograph Scientific).

Synapse Immunolabeling, Spectral Imaging, and Three-Dimensional Analysis: After fixation in 4% formaldehyde, prepared from fresh paraformaldehyde, dissociated hippocampal cultures were incubated for 10 min with 0.1 M glycine in PBS 1× to mask free aldehyde groups, thus preventing unspecific antibodies binding. Permeabilization was performed as described above (see Immunocytochemistry and Fluorescent Microscopy). Samples were subsequently incubated with primary antibodies for 30 min at 37 °C, 5% CO₂, 95% relative humidity, and after being washed with PBS 1×, with secondary antibodies for 45 min. Mounting was performed with antifade medium Fluoromount (Sigma-Aldrich) on 0.17 μm-thick microscope glass slides. Neurons were stained through anti-β-tubulin III primary antibody (1:800, Sigma-Aldrich) and visualized with Alexa 594 antirabbit in goat as the secondary antibody (1:800, Invitrogen). Synapses were instead labeled with mouse anti-Bassoon/BSN primary monoclonal antibody (1:400, Abcam) and visualized with Alexa 488 antimouse in goat as the secondary antibody (1:800, Invitrogen). Nuclei were stained with DAPI (1:800, Invitrogen). Spectral images (2048 × 2048 pixels) acquisition in variable bandpass mode was carried out with the AIR confocal system mounted on a Nikon Eclipse Ti2 inverted microscope (60× plan apo λ oil, 1.40 NA). The selected bandpass (10 nm steps) for the aforementioned RGB channels were respectively 590–610 nm (R), 510–530 nm (G), and 450–470 nm (B). Line averaged scans (Ø × 2) were used to further increase signal-to-noise ratio, and six to eight stacks of 700 nm were sufficient to reconstruct neuronal structures and synaptic clusters. 3D image analysis was performed with NIS-Elements AR Analysis software (version 5.20.02, Nikon Instruments); through the 3D object measurement function, it was possible to define a common intensity threshold of 36-bit images for red and green channels. The total volumes corresponding to β-tubulin III⁺ and Bassoon⁺ structures were evaluated as the sum of connected and contiguous marked objects. The ratio between these volumes allowed the authors to consistently compare the

fraction of neuronal volume occupied by synaptic clusters in cultures grown onto flat versus nanostructured surfaces.

Electrical Stimulation: To perform extracellular stimulation through PS-CNT-NP substrates, a 4 mm × 4 mm square piece of sample was glued on a glass coverslip (16 mm in diameter and 0.22 mm in thickness) with a 1 mm hole drilled at its center, allowing contacting the back of the conductive sample electrically. PDMS was used to mount the sample leaving its central part, where the electrode contact was placed, PDMS-free. The glass slide hole was subsequently filled with a small drop of silver paste (Sigma Aldrich) to assure good conductivity and increase sample robustness (curing time 30 min at 60 °C). The PS-CNT-PS sample mounted on the glass slide was subsequently glued on a custom made liquid cell for neuronal extracellular stimulation. The latter was obtained drilling an 8 mm-diameter hole in the bottom of a 35 mm PS petri dish (Falcon).^[42] To ensure neuronal viability and avoid medium leak during culture the sample assembly was mounted on the petri dish hole using PDMS silicone elastomer (Sylgard 184, Dow Corning Co.).^[37] This assembly offered easy access for the stimulating electrode to contact in a dry environment the PS-CNT NPs from the bottom side (see the sketch in Figure 5A). Cultures were grown for 10 DIV in the same conditions described above (see Experimental Section, Primary Cultures). Cells were loaded with the Ca²⁺ dye, and after incubation, the petri dish with the substrate was mounted in a fixed-stage upright microscope (Eclipse FN1, Nikon), and it was used as a perfusion chamber during the experiment (see Experimental Section, calcium imaging). Spontaneous calcium transients were recorded with a 20× water immersion objective (UMPlanFL, 0.5 NA, Olympus) using an EMCCD camera (iXon Ultra 897, Andor, Oxford Instruments) controlled by a computer through NIS-Elements D (Nikon). Images were acquired at a sampling rate of 6.67 Hz (150 ms exposure time) under continuous illumination.

After ≈10 min of spontaneous activity, the application of the synaptic blockers (all from Sigma-Aldrich) APV 25 μM (NMDA receptor selective antagonist), bicuculline 10 μM (GABA_A receptor antagonist), and CNQX 10 μM (AMPA/kainate receptor antagonist) completely silenced the network, as previously reported.^[43] In these conditions, only evoked signals were visible in a Ca²⁺ imaging experiment.^[44] The positive output of an external insulated stimuli generator (Digitimer DS2A) was connected to a stimulating platinum wire contacting the PS-CNT-NP substrate from its bottom side. In contrast, the negative output was plugged into an Ag/AgCl pellet electrode submerged in the extracellular saline solution (Figure 5A). The authors therefore manually triggered the voltage pulse train through the isolated stimulator, tuning stimuli according to literature guidelines.^[40,52] Analysis was accomplished with ImageJ software (NIH) and Clampfit software (pClamp suite, 10.4 version; Axon Instruments) in off-line mode.

Organotypic Slice Cultures: Spinal cord slices were obtained from embryos at 12–13 days of gestation (E12–E13) from a pregnant female mouse (C57Bl/6), as previously reported.^[53] All procedures were approved by the local veterinary authorities and performed in accordance with the Italian law (decree 26/14) and the UE guidelines (2007/526/CE and 2010/63/UE). The animal use was approved by the Italian Ministry of Health (22DABNTWO). All efforts were made to minimize suffering and to reduce the number of animals used. Pregnant mice were sacrificed by CO₂ overdose and beheading; fetuses were finally extracted by cesarean section. The spinal cord's thoracolumbar portion was explanted and cut into transversal slices (275 μm) with a tissue chopper (McIlwain TC752, Campden Instruments Ltd.). Slices were dissected from the surrounding tissue and plated either onto glass coverslips or the tested materials (PS-NP and PS-CNT-NP) by clotting 15 μL of chicken plasma with 23 μL of thrombin (both from Sigma-Aldrich). Organotypic spinal cords were therefore grown with 1 mL medium containing 66% DMEM 1× (Gibco), 8% sterile water for tissue culture, 25% fetal bovine serum (Gibco), 1% antibiotic-antimycotic (Gibco), 2% B-27 supplement (Gibco), and 20 ng mL⁻¹ nerve growth factor (NGF, Alomone Laboratories); 300 mOsm; pH 7.35. Cultures were kept in a roller drum (120 revs/min, at 37 °C and 5% CO₂) for ≈14–21 days in vitro (DIV).^[45,46,51] After 7 DIV, culture medium was replaced for 24 h by fresh

medium containing antimitotics (10 μM ARA-C/Uridine/5-Fluorouracil) and reduced NGF concentration (5 ng mL⁻¹). At 8 DIV, fresh medium with reduced NGF was added and refreshed every 7 days.

Organotypic Culture Immunofluorescence and Confocal Microscopy: Organotypic slices were fixed in 4% formaldehyde, prepared from fresh paraformaldehyde, in PBS 1× for at least 1 h. After fixation, slices were incubated for 10 min with 0.1 M glycine in PBS 1× and permeabilized for 1 h with 0.3% Triton-X-100 (Carlo Erba) in PBS 1× added with 5% FBS (Gibco) and 4% BSA (Sigma-Aldrich) to prevent non-specific binding of primary antibodies. Samples were subsequently incubated with primary antibodies overnight at 4 °C and with the secondary antibodies for 2 h at room temperature (three washes in PBS 1× preceded each step). Mounting was performed with antifade medium Fluoromount (Sigma-Aldrich) on 1 mm-thick microscope glass slides. All neurons were labeled through anti-β-tubulin III primary antibody (1:800, Sigma-Aldrich) and visualized with Alexa 594 antirabbit in goat as the secondary antibody (1:800, Invitrogen). Exclusive staining of motoneurons was instead achieved with antineurofilament H (SMI-32, 1:800, Biologend) recognized by Alexa 488 antimouse in goat as the secondary antibody (1:800, Invitrogen). Nuclei were stained with DAPI (1:500, Invitrogen). A Nikon Eclipse Ti2 inverted microscope connected to an A1R confocal system (Nikon Instruments) was used to acquire stitched images (10× Plan Apo λ, 0.45 NA) to obtain a morphological insight of the stained spinal cord slice cultures.

Spinal Cord Calcium Imaging: Organotypic spinal cord samples, grown in vitro for 2–3 weeks, were loaded with cell-permeable Ca²⁺ dye Fluo-4 AM (Molecular Probes); 11.6 μL of DMSO (Sigma-Aldrich) was added to the stock 50 μg of the dye, and cultures were incubated with a final concentration of 4 μM for 1 h in the roller drum at 37 °C, 5% CO₂. After dye loading, a de-esterification period followed, cultures were maintained in extracellular saline solution (described above) in the same incubator for 30 min. Samples were mounted on the previously described inverted microscope (Nikon Eclipse Ti-U). The dye was excited at 488 nm, and the emission was detected at 520 nm. Cultures were continuously perfused with extracellular saline solution, and neurons at the premotor region in the slice's ventral zone were observed with a 40× objective (PlanFluor, 0.60 NA). Images were acquired every 150 ms using the ORCA-Flash4.0 V2 sCMOS camera (Hamamatsu) operating at binning 4. After cultures accustomed to the extracellular solution, spontaneous activity was recorded for 10 min. 25 μM bicuculline (GABA_A antagonist; Sigma-Aldrich) and 2 μM strychnine (glycine receptor antagonist; Sigma-Aldrich) were subsequently perfused for 20 min to weaken the synaptic inhibition and increase the synchronization. Finally, 1 μM TTX (a voltage-gated, fast Na⁺ channel blocker; Latoxan) was added to confirm the recorded signals' neuronal nature. Images were analyzed with ImageJ software (NIH), and the corresponding traces were extracted with Clampfit software (pClamp suite, 10.4 version; Axon Instruments) in off-line.

Statistical Analysis: Statistical analysis was accomplished using Prism 6 software (GraphPad): datasets normality was addressed with D'Agostino and Pearson omnibus normality test. Non-parametric tests were used in both non-normally distributed data and unequal variances among tested data sets. Accordingly, statistics between two independent samples were performed with *t*-test or Mann–Whitney U test. In contrast, three independent samples' differences were tested with either one-way ANOVA adjusted for multiple comparisons with Tukey's correction or Kruskal–Wallis test adjusted with Dunn's multiple comparison test. All data were plotted as median with their 25th (1st quartile, Q₁) and 75th (3rd quartile, Q₃) percentiles, with whiskers representing 10th and 90th percentiles. Descriptive statistics used in the text express the central tendency as mean ± SD for normal distributions and median for non-normal distributions.

Supporting Information

Supporting Information is available from the Wiley Online Library or from the author.

Acknowledgements

This work was performed within the framework of the ByAXON project funded by the European Union's Horizon 2020 FET Open program under grant agreement No. 737116. The work was partially funded by the Spanish Ministry of Science and Innovation through project BiSURE (Grant DPI2017-90058-R) and the "Severo Ochoa" Programme for Centres of Excellence in R&D (MINECO, Grant SEV-2016-0686). D.S. acknowledges the support of the European Union's Horizon 2020 research and innovation program under the Marie Skłodowska-Curie grant agreement no. 838902. M. A. Monclús and J. M. Molina-Aldareguia from IMDEA Materials are acknowledged for the nanoindentation testing.

Conflict of Interest

The authors declare no conflict of interest.

Data Availability Statement

The data that support the findings of this study are available from the corresponding author upon reasonable request.

Keywords

biomaterials, carbon nanotubes, electrical stimulation, hippocampal cultures, nanopillars, spinal cord organotypic slices, suspended two-dimensional cultures

Received: December 7, 2020

Revised: January 26, 2021

Published online:

- [1] D. Scaini, L. Ballerini, *Curr. Opin. Neurobiol.* **2018**, *50*, 50.
- [2] T. Dvir, B. P. Timko, D. S. Kohane, R. Langer, *Nat. Nanotechnol.* **2011**, *6*, 13.
- [3] S. G. Higgins, M. Becce, A. Belessiotis-Richards, H. Seong, J. E. Sero, M. M. Stevens, *Adv. Mater.* **2020**, *32*, 1903862.
- [4] W. Kim, J. K. Ng, M. E. Kunitake, B. R. Conklin, P. Yang, *J. Am. Chem. Soc.* **2007**, *129*, 7228.
- [5] F. Viela, D. Granados, A. Ayuso-Sacido, I. Rodríguez, *Adv. Funct. Mater.* **2016**, *26*, 5599.
- [6] C. Xie, L. Hanson, W. Xie, Z. Lin, B. Cui, Y. Cui, *Nano Lett.* **2010**, *10*, 4020.
- [7] L. Micholt, A. Gärtner, D. Prodanov, D. Braeken, C. G. Dotti, C. Bartic, *PLoS One* **2013**, *8*, e66170.
- [8] J. Seo, J. Kim, S. Joo, J. Y. Choi, K. Kang, W. K. Cho, I. S. Choi, *Small* **2018**, *14*, 1801763.
- [9] C. J. Bettinger, R. Langer, J. T. Borenstein, *Angew. Chem., Int. Ed.* **2009**, *48*, 5406.
- [10] N. W. S. Kam, E. Jan, N. A. Kotov, *Nano Lett.* **2009**, *9*, 273.
- [11] L. Amato, A. Heiskanen, C. Caviglia, F. Shah, K. Zór, M. Skolimowski, M. Madou, L. Gammelgaard, R. Hansen, E. G. Seiz, M. Ramos, T. R. Moreno, A. Martínez-Serrano, S. S. Keller, J. Ennéus, *Adv. Funct. Mater.* **2014**, *24*, 7042.
- [12] A. Asif, S. García-López, A. Heiskanen, A. Martínez-Serrano, S. S. Keller, M. P. Pereira, J. Ennéus, *Adv. Healthcare Mater.* **2020**, *9*, 2001108.
- [13] A. T. Nguyen, S. R. Sathe, E. K. F. Yim, *J. Phys.: Condens. Matter* **2016**, *28*, 183001.
- [14] M. Marcus, K. Baranes, M. Park, I. S. Choi, K. Kang, O. Shefi, *Adv. Healthcare Mater.* **2017**, *6*, 1700267.
- [15] V. Gautam, S. Naureen, N. Shahid, Q. Gao, Y. Wang, D. Nisbet, C. Jagadish, V. R. Daria, *Nano Lett.* **2017**, *17*, 3369.
- [16] J. T. Robinson, M. Jorgolli, A. K. Shalek, M. H. Yoon, R. S. Gertner, H. Park, *Nat. Nanotechnol.* **2012**, *7*, 180.
- [17] K. Kang, Y.-S. Park, M. Park, M. J. Jang, S.-M. Kim, J. Lee, J. Y. Choi, D. H. Jung, Y.-T. Chang, M.-H. Yoon, J. S. Lee, Y. Nam, I. S. Choi, *Nano Lett.* **2016**, *16*, 675.
- [18] K. Tybrandt, D. Khodagholy, B. Dielacher, F. Stauffer, A. F. Renz, G. Buzsáki, J. Vörös, *Adv. Mater.* **2018**, *30*, 1706520.
- [19] C. Nick, S. Quednau, R. Sarwar, H. F. Schlaak, C. Thielemann, *Microsyst. Technol.* **2014**, *20*, 1849.
- [20] J. W. Salatino, K. A. Ludwig, T. D. Y. Kozai, E. K. Purcell, *Nat. Biomed. Eng.* **2017**, *1*, 862.
- [21] C. Vallejo-Giraldo, K. Krukiewicz, I. Calaresu, J. Zhu, M. Palma, M. Fernandez-Yague, B. McDowell, N. Peixoto, N. Farid, G. O'Connor, L. Ballerini, A. Pandit, M. J. P. Biggs, *Small* **2018**, *14*, 1800863.
- [22] J. J. Hernández, M. A. Monclús, I. Navarro-Baena, F. Viela, J. M. Molina-Aldareguia, I. Rodríguez, *Sci. Rep.* **2017**, *7*, 1.
- [23] H. I. Lin, S. W. Kuo, T. J. Yen, O. K. Lee, *Sci. Rep.* **2018**, *8*, 12913.
- [24] A. Mazzatenta, M. Giugliano, S. Campidelli, L. Gambazzi, L. Businaro, H. Markram, M. Prato, L. Ballerini, *J. Neurosci.* **2007**, *27*, 6931.
- [25] V. Lovat, D. Pantarotto, L. Lagostena, B. Cacciari, M. Grandolfo, M. Righi, G. Spalluto, M. Prato, L. Ballerini, *Nano Lett.* **2005**, *5*, 1107.
- [26] W. J. Polackcheck, C. S. Chen, *Nat. Methods* **2016**, *13*, 415.
- [27] J. Lantoine, T. Grevesse, A. Villers, G. Delhay, C. Mestdagh, M. Versaavel, D. Mohammed, C. Bruyère, L. Alaimo, S. P. Lacour, L. Ris, S. Gabriele, *Biomaterials* **2016**, *89*, 14.
- [28] D. M. Suter, K. E. Miller, *Prog. Neurobiol.* **2011**, *94*, 91.
- [29] M. Chighizola, T. Dini, C. Lenardi, P. Milani, A. Podestà, C. Schulte, *Biophys. Rev.* **2019**, *11*, 701.
- [30] S. M. Kim, S. Lee, D. Kim, D. H. Kang, K. Yang, S. W. Cho, J. S. Lee, I. S. Choi, K. Kang, M. H. Yoon, *Nano Res.* **2018**, *11*, 2532.
- [31] C. A. R. Chapman, H. Chen, M. Stamou, J. Biener, M. M. Biener, P. J. Lein, E. Seker, *ACS Appl. Mater. Interfaces* **2015**, *7*, 7093.
- [32] A. E. Hampe, Z. Li, S. Sethi, P. J. Lein, E. Seker, *Nanomaterials* **2018**, *8*, 452.
- [33] P. Moshayedi, G. Ng, J. C. F. Kwok, G. S. H. Yeo, C. E. Bryant, J. W. Fawcett, K. Franze, J. Guck, *Biomaterials* **2014**, *35*, 3919.
- [34] M. J. P. Biggs, R. G. Richards, M. J. Dalby, *Nanomedicine* **2010**, *6*, 619.
- [35] N. P. Pampaloni, D. Scaini, F. Perissinotto, S. Bosi, M. Prato, L. Ballerini, N. Paolo, D. Scaini, F. Perissinotto, S. Bosi, M. Prato, L. Ballerini, *Nanomedicine* **2018**, *14*, 2521.
- [36] M. Giugliano, P. Darbon, M. Arsiero, H. R. Lüscher, J. Streit, *J. Neurophysiol.* **2004**, *92*, 977.
- [37] S. Bosi, R. Rauti, J. Laishram, A. Turco, D. Lonardonì, T. Nieuw, M. Prato, D. Scaini, L. Ballerini, *Sci. Rep.* **2015**, *5*, 9562.
- [38] N. P. Pampaloni, M. Lottner, M. Giugliano, A. Matruggio, F. D'Amico, M. Prato, J. A. Garrido, L. Ballerini, D. Scaini, *Nat. Nanotechnol.* **2018**, *13*, 755.
- [39] K. D. Micheva, B. Busse, N. C. Weiler, N. O'Rourke, S. J. Smith, *Neuron* **2010**, *68*, 639.
- [40] D. R. Merrill, M. Bikson, J. G. R. R. Jefferys, *J. Neurosci. Methods* **2005**, *141*, 171.
- [41] I. Rago, R. Rauti, M. Bevilacqua, I. Calaresu, A. Pozzato, M. Cibinel, M. Dalmiglio, C. Tavagnacco, A. Goldoni, D. Scaini, *Adv. Biosyst.* **2019**, *3*, 1800286.
- [42] A. Domínguez-Bajo, B. L. Rodilla, I. Calaresu, A. Arché-Núñez, A. González-Mayorga, D. Scaini, L. Pérez, J. Camarero, R. Miranda,

- E. López-Dolado, M. T. González, L. Ballerini, M. C. Serrano, *Adv. Biosyst.* **2020**, *4*, 2000117.
- [43] I. Breskin, J. Soriano, E. Moses, T. Tlusty, *Phys. Rev. Lett.* **2006**, *97*, 8102.
- [44] S. Stern, A. Agudelo-Toro, A. Rotem, E. Moses, A. Neef, *PLoS One* **2015**, *10*, e0132577.
- [45] D. Avossa, M. D. Rosato-Siri, F. Mazzarol, L. Ballerini, *Neuroscience* **2003**, *122*, 391.
- [46] S. Sibilla, A. Fabbro, M. Grandolfo, P. D'Andrea, A. Nistri, L. Ballerini, *Eur. J. Neurosci.* **2009**, *29*, 1543.
- [47] M. Galante, A. Nistri, L. Ballerini, *J. Physiol.* **2000**, *523*, 639.
- [48] M. Grumet, G. M. Edelman, *J. Cell Biol.* **1988**, *106*, 487.
- [49] V. Onesto, L. Cancedda, M. L. Coluccio, M. Nanni, M. Pesce, N. Malara, M. Cesarelli, E. D. Fabrizio, F. Amato, F. Gentile, *Sci. Rep.* **2017**, *7*, 9841.
- [50] S.-H. Park, J. Bae, *Recent Pat. Nanotechnol.* **2017**, *11*, 109.
- [51] S. Usmani, E. R. Aurand, M. Medelin, A. Fabbro, D. Scaini, J. Laishram, F. B. Rosselli, A. Ansuini, D. Zoccolan, M. Scarselli, M. D. Crescenzi, S. Bosi, M. Prato, L. Ballerini, *Sci. Adv.* **2016**, *2*, e1600087.
- [52] M. A. Meza-Cuevas, in *Simulation of Neurons by Electrical Means*, (Ed: W. Krautschneider), Logos Verlag, Berlin **2015**.
- [53] A. Fabbro, A. Villari, J. Laishram, D. Scaini, F. M. Toma, A. Turco, M. Prato, L. Ballerini, *ACS Nano* **2012**, *6*, 2041.